Chen, Yuzhu; Hua, Huilian; Wang, Jun; Lund, Peter D.

Thermodynamic performance analysis and modified thermo-ecological cost optimization of a hybrid district heating system considering energy levels

Published in:
Energy

DOI:
10.1016/j.energy.2021.120067

Published: 01/06/2021

Document Version
Peer-reviewed accepted author manuscript, also known as Final accepted manuscript or Post-print

Journal Pre-proof

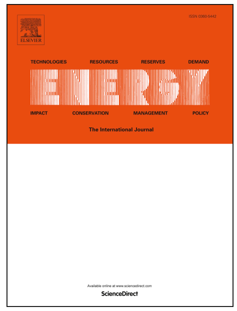

Thermodynamic performance analysis and modified thermo-ecological cost optimization of a hybrid district heating system considering energy levels

Yuzhu Chen, Huilian Hua, Jun Wang, Peter D. Lund

PII: S0360-5442(21)00316-9

DOI: https://doi.org/10.1016/j.energy.2021.120067

Reference: EGY 120067

To appear in: *Energy*

Received Date: 17 August 2020

Revised Date: 2 February 2021

Accepted Date: 4 February 2021

Please cite this article as: Chen Y, Hua H, Wang J, Lund PD, Thermodynamic performance analysis and modified thermo-ecological cost optimization of a hybrid district heating system considering energy levels, *Energy*, https://doi.org/10.1016/j.energy.2021.120067.

Yuzhu Chen: Methodology, Software, Data curation,

Huilian Hua: Writing- Original draft preparation

Jun Wang: Software, Validation

Peter D. Lund: Writing- Reviewing and Editing

Thermodynamic performance analysis and modified thermo-ecological cost optimization of a hybrid district heating system considering energy levels

Yuzhu Chen, Huilian Hua, Jun Wang*, Peter D. Lund [a, b*]

[a] Key Laboratory of Solar Energy Science and Technology in Jiangsu Province, Southeast University, No 2 Si Pai Lou, Nanjing, 210096, China

[b] School of Science, Aalto University, P.O. Box 15100, FI-00076, Aalto (Espoo), Finland

Yuzhu Chen (First author):

Affiliation: Key Laboratory of Solar Energy Science and Technology in Jiangsu Province, Southeast University, No 2 Si Pai Lou, Nanjing, 210096, China;

e_mail: 230208510@seu.edu.cn

Huilian Hua (Second author):

Affiliation: Key Laboratory of Solar Energy Science and Technology in Jiangsu Province, Southeast University, No 2 Si Pai Lou, Nanjing, 210096, China;

e_mail: huilianhua98@163.com

Jun Wang (Corresponding author):

Affiliation: Key Laboratory of Solar Energy Science and Technology in Jiangsu Province, Southeast University, No 2 Si Pai Lou, Nanjing, 210096, China;

e_mail: 101010980@seu.edu.cn

Peter D. Lund, (Corresponding author):

Affiliation: School of Science, Aalto University, P.O. Box 15100, FI-00076, Aalto (Espoo), Finland;

e_mail: peter.lund@aalto.fi

Graphical abstract

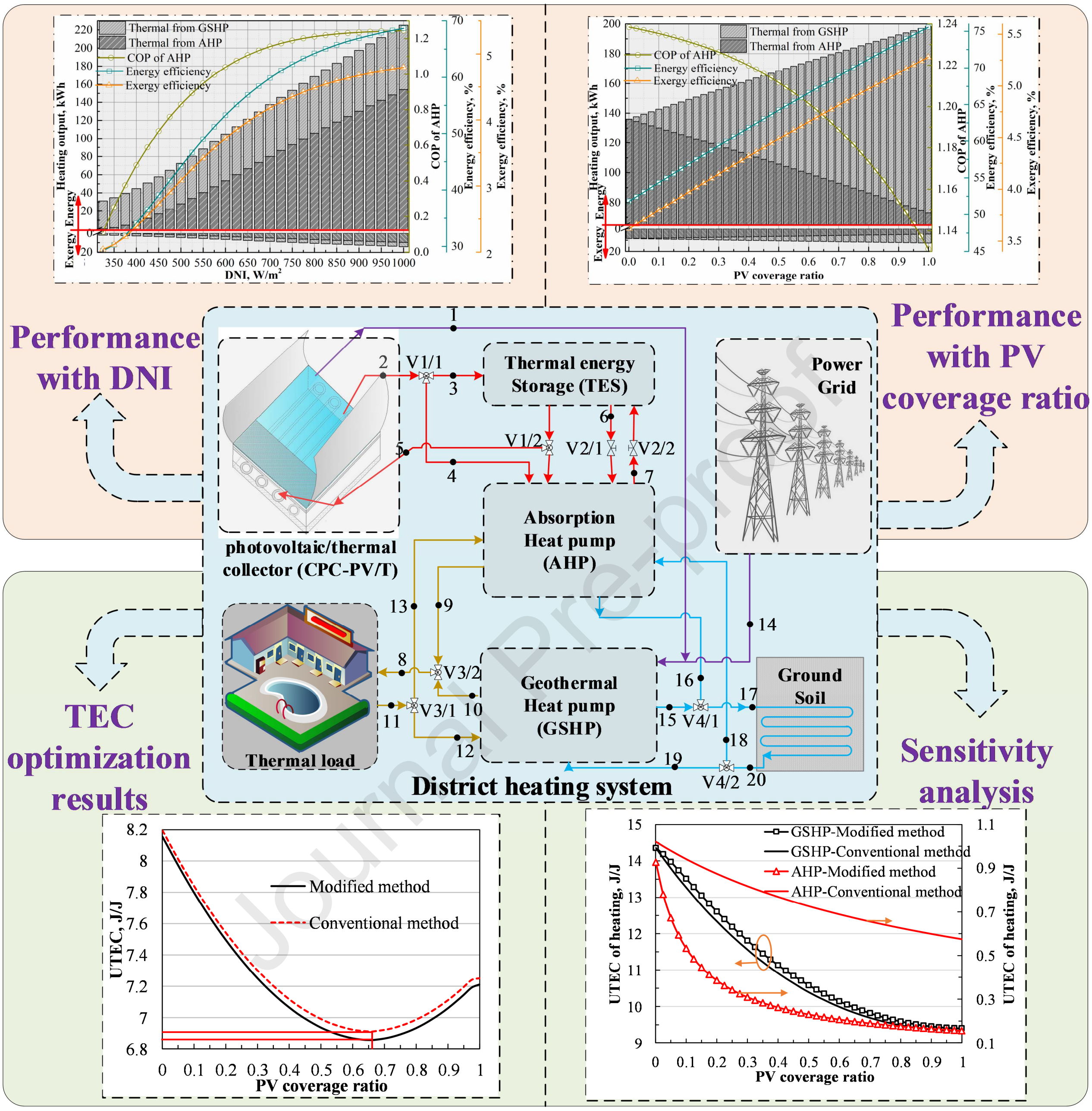

Thermodynamic performance analysis and modified thermo-ecological cost optimization of a hybrid district heating system considering energy levels

Yuzhu Chen, Huilian Hua, Jun Wang*, Peter D. Lund [a, b*]

[a] Key Laboratory of Solar Energy Science and Technology in Jiangsu Province, Southeast University, No 2 Si Pai Lou, Nanjing, 210096, China

[b] School of Science, Aalto University, P.O. Box 15100, FI-00076, Aalto (Espoo), Finland

∗ Corresponding authors: Jun Wang; e-mail: 101010980@seu.edu.cn; Peter D. Lund: e-mail: peter.lund@aalto.fi

Abstract

Utilization of the renewable resources in district heating systems can reduce the use of fossil fuels, operating costs and protect the environment. In this study, an integrated hybrid system consisting of concentrating photovoltaic/thermal collectors (PV/T), geothermal (GSHP) and absorption (AHP) heat pumps is considered for district heating. The thermodynamic performance of the system at various conditions is explored through detailed simulations. A modified thermo-ecological cost (TEC) method is used to optimize the structure of the PV/T by considering contributions of different flows. The results show that a higher solar irradiance level and a higher PV coverage ratio have a positive impact on the thermal performance of the hybrid system. The TEC-based optimization shows that a 66% PV coverage ratio of PV/T yields a minimum thermo-ecological heating cost of 6.86 J/J, which is slightly lower than cost with a conventional method. Based on the sensitivity analysis, other key parameters except the operating time and the PV coverage ratio have a negative influence on the economic performance of the district heating system, because of the increasing cumulative exergy consumption of the GSHP or PV/T.

Keywords: photovoltaic/thermal collectors, district heating system, geothermal heat pump, thermodynamic performance, modified thermo-ecological optimization

Nomenclature

AHP	Absorption heat pump
CExE	Cumulative exergy consumption
COP	Coefficient of performance
CPC	Compound parabolic concentrator
EES	Engineering equation solver
GSHP	Geothermal heat pump
PV/T	Photovoltaic/thermal collector
TEC	Thermo-ecological cost
TES	Thermal energy storage
UTEC	Unit thermo-ecological cost

Symbols

a	Exergy consumption of process, kWh
A	Area, m^2
b	Breath of receiver, m
$\dot{b}$	Exergy consumption of non-renewable resource, kWh
c	Specific heat, J/(kg K)
DNI	Direct normal irradiance, W/m^2
E	Electricity, kWh
EL	Energy level
F'	Collector efficiency factor
h	Enthalpy, kJ/(kg K)
h_{pf}	Heat transfer coefficient between fluid and plate, $W/(m^2\ K)$

L	Operation times, hour
$LMTD$	logarithmic mean temperature difference
m	Mass flow, kg/s
n	Variable coefficient
p	Pollutant emissions, kg
PF	Penalty factor
Q	Energy, kWh
T	Temperature, °C
R	Ideal gas constant
S	Entropy, J/k
t	Time, s
U	Heat transfer coefficient, W/(m^2 k)
V	Volume, m^3
χ	Temperature coefficient of PV efficiency
ς	Concentration of LiBr solution
ρ	Density, kg/m^3
η	Efficiency, %
ξ	Compensation cost, kWh/kg
ε	Ratio
π	Concentrating efficiency of CPC
τ_g	Transmissivity of glass
α	Absorptivity

Superscript/ Subscript

a	Ambient
ab	Absorber
c/cell/m/PV	Solar cell
co	Condenser
com	Compressor
en	Energy
eva	Evaporator
ex	Exergy
f	Fluid water
g	Generator
ini	Initial cost
k	k^{th} pollutant
oper	Operation
ou/in	Outlet/inlet
p	Absorber plate
pri	Primary energy
r	r^{th} hour
s	s^{th} non-renewable resource
th	Throttle valve

1. Introduction

District heating systems can reduce fossil fuel consumption and emissions by utilizing local renewable resources [1]. Among the various renewable sources, solar heating is a promising technology, which can reach cost-effectiveness in several places [5]. There are different types of solar collectors available for solar heating such as evacuated tube collectors [2], flat plat collectors [3], and parabolic trough collectors [4].

The intermittency of solar radiation often hampers the wider use of these systems [5]. Therefore, to overcome the demand and supply mismatch, solar heating systems can be integrated with other energy technologies such as heat pumps [6], which not only provide a more continuous heat output, but also upgrade the quality of solar heat [7]. In direct-expansion heat pump systems, the solar collectors can directly work as the evaporator of heat pump enabling continuous operation [8]. Solar heating systems are can also be used complimentary to heat pump systems [9, 10]. As heat pumps need electricity, connecting these to photovoltaic/thermal collectors (PV/T) would also be an interesting option to reduce the grid electricity consumption [11]. Typically, ground-coupled heat pump systems (GSHP) would need less electricity than e.g. air heat pumps due to higher energy performance [12]. In this study, the focus will be on the PV/T and GSHP. This kind of system concept represents new direction in district heating.

Previous work on similar systems has included their performance and thermodynamic modelling [13, 14] and different economic [15] and techno-economic [16] analyses. Life cycle assessments of GSHP coupled to PV/T [17, 18] showed that the life-cycle cost of heating could be decreased by almost 20% over a service life of 20 years. Dual mode systems in which the solar heating produces the hot water and preheats the heat pump evaporator during the heating season have also been proposed [19] to increase the system performance.

There are different approaches to evaluate the performance of such systems. Among the evaluation indicators [20], the thermo-ecological cost (TEC) indicator considers the specific process from an ecological point of view by determining the cumulative exergy consumption (CExE). The basis of the TEC method has been presented in [21, 22] and it has recently been applied to fossil fuels [23], renewable resources [24] including solar [25] and wind power [26]. TEC has also been used to analyze the performance of advanced energy systems such as combined cooling, heating, and power systems [27], fuel combustion power plant [28], and LNG-driven Stirling engines [29]. However, in such conventional TEC analyses, the contribution of different components and flows are seldom considered.

This study is extended from previous work [30] by not only employing thermodynamic criteria to assess the thermal performance of the proposed system, but also optimizing the PV-to-thermal ratio of the PV/T device, which is the central component in the present concept, using the modified thermo-ecological method. Original contributions in the paper include the following:

(1) A novel hybrid system is proposed, which integrates PV/T, geothermal and absorption heat pumps to utilize local renewable sources effectively;

(2) The original thermo-ecological method is modified by considering the energy grades of the multiply products;

(3) The modified TEC method is used to optimize the PV coverage ratio of the PV/T unit with comparison to conventional methods;

(4) A sensitivity analysis against key parameters is also presented.

The paper is divided as follows: Section 2 describes the hybrid system and its thermal models; Section 3 describes the evaluation indicators and the modified TEC method; Section 4 presents the key results from the thermodynamic analysis and the TEC optimization; Section 5 summarizes some crucial conclusions.

2. District heating system

The hybrid heating system including the energy flowcharts and the thermal models are described in the next.

2.1 Parameters of building

A sample office building with 500 m^2 rooftop area in Beijing (a cold region in China) is selected as the case building for the analyses. The weather parameters (year 2015) are searched in Energy Plus software [31]. The office building is operated from 8 am to 8 pm on weekdays. The person density is 0.1 persons per square meter. The total height of the building is almost 11m and the ceiling height is 3.6m. 30% of the wall area is covered by the windows and glazing [32]. A mean setpoint temperature of 16°C is used as shown in Fig. 1 [32]. The DesT software [33] is employed to simulate the hourly heating load shown in Fig. 1. The peak heating load is 300 kW.

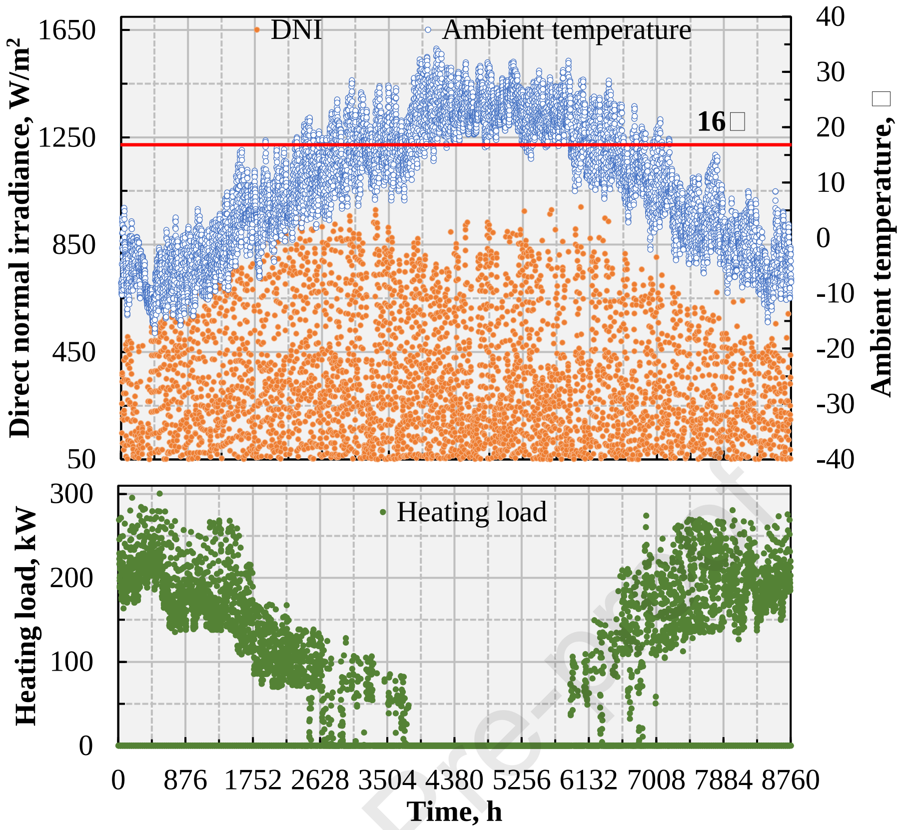

Fig. 1. Sample weather data and space heating load of an office building in Beijing (Weather data is for 2015 and source from https:www.energyplus.net [31]).

2.2 Energy flowcharts of the system

The flows of the heating system are shown in Fig. 2. The system includes a Compound Parabolic Concentrator (CPC)-PV/T and AHP, GSHP, and TES units [30].

In the CPC-PV/T, the direct normal irradiance (DNI) is converted into electricity by the PV module, while the extra heat is absorbed by the thermal collectors placed behind. The solar thermal output is utilized to heat the hot water (80°C, state 5). After releasing heat in the thermal tank (state 3, TES) and in the absorption heat pump (state 4, AHP) by controlling the valve V1/1, the returned water is fed back to the PV/T for the next cycle.

Based on the working principle of the AHP [34], the space heating water is primarily generated by absorbing the heat from the solar hot water (state 4) and the geothermal water (state 18). During low irradiance or high heating load conditions, the GSHP [35] (state 1 or 14) is employed using geothermal water as heat source (state 19). It should be pointed out that the solar electricity cannot be fed into the grid meaning that during high irradiance conditions some solar electricity could be wasted. The integration of the individual components of the hybrid system is relatively complex and its parameters need to be adjusted for cost-effective operation.

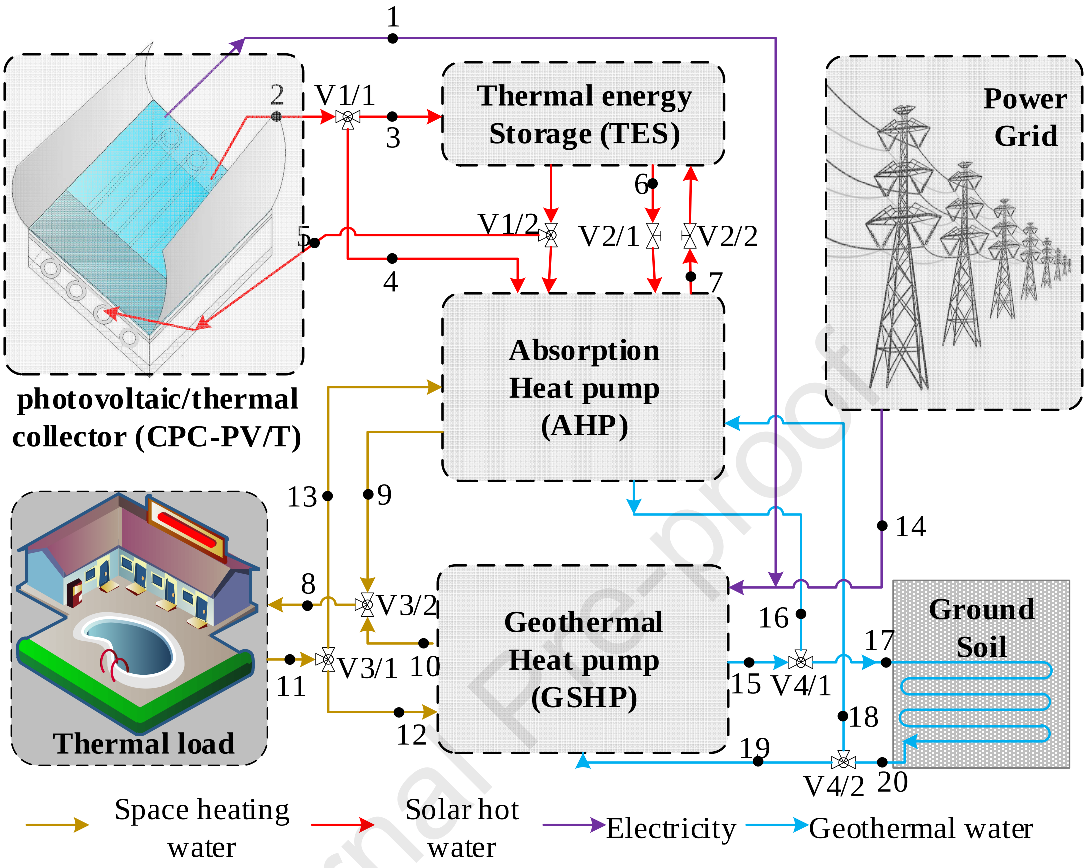

Fig. 2. Energy flows of the proposed heating system [30].

2.3 Models and validation

All mathematical models including the CPC-PV/T [36], AHP [34], TES [37], and GSHP [35] are constructed with the Engineering Equation Solver (EES) [38] software.

2.3.1 Photovoltaic/thermal collector

The PV/T unit shown in Fig.3 simultaneously produces solar electricity and thermal energy. For the performance simulation some assumptions are used: the collector is at the steady state, the temperature differences collector insolation and in the PV module are ignored. The PV/T system model has been described in [39].

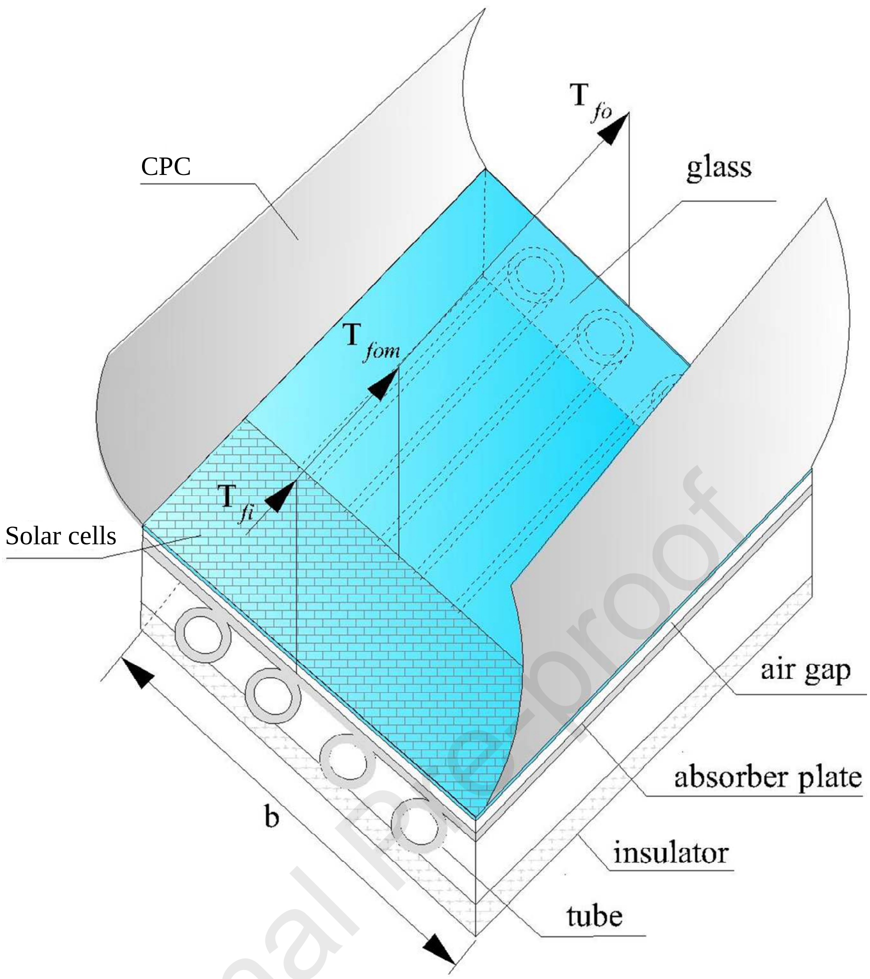

Fig. 3 Structure of the CPC-PVT with 25% PV coverage ratio [36].

The energy balance equation of the PV cells can be expressed as follows:

$$\pi \cdot \alpha_c \cdot \tau_g \cdot \beta_c \cdot DNI \cdot A_{am} = [U_{tc,a} \cdot (T_c - T_a) + U_{tc,p} \cdot (T_c - T_p)] \cdot A_{rm} + \pi \cdot \eta_m \cdot DNI \cdot A_{am} \quad (1)$$

where π is the Intercept factor of the CPC, α_c is the absorptivity of the solar cell, τ_g is the transmissivity of glass, β_c is the concentration ratio of CPC, DNI is the direct normal irradiance, η_m is the electrical efficiency of PV module. A_{am} and A_{rm} are the areas of the aperture covered by the PV module and receiver covered by the PV module, respectively. $U_{tc,a}$ and $U_{tc,p}$ are the overall heat transfer coefficients of the cell to ambient and cell to plate, respectively. T_c, T_a and T_p are the solar cell temperature, ambient temperature and absorber plate temperature, respectively.

The solar cell temperature can be calculated as:

$$T_{cell} = \frac{(\alpha\tau)_{1,eff} + U_{tc,a} \cdot T_a + U_{tc,p} \cdot T_p}{U_{tc,a} + U_{tc,p}} \tag{2}$$

where $(\alpha\tau)_{1,eff}$ is the product of effective absorptivity of the solar cell and the transmittivity of the covered glass.

The energy balance of the absorber plate below the PV module is expressed as:

$$\pi \cdot \alpha_P \cdot \tau_g^2 \cdot (1-\beta_c) \cdot DNI \cdot A_{am} + U_{t,cp}(T_c - T_p) \cdot A_{rm} = F' \cdot h_{pf} \cdot (T_p - T_f) \cdot A_{rm} + U_{t,pa} \cdot (T_p - T_f)] \cdot A_{rm} + \pi \cdot \eta_m \cdot DNI \cdot A_{am} \tag{3}$$

where α_p is the absorptivity of absorber plate, $U_{tp,a}$ is the heat transfer coefficient between the plate and the ambient without the PV area, F' is the collector efficiency factor and h_{pf} is the heat transfer coefficient between the absorber plate and water.

The absorber plate temperature can be expressed as:

$$T_P = \frac{[(\alpha\tau)_{2,eff} + PF_1 \cdot (\alpha\tau)_{1,eff}] \cdot DNI + U_{L2} \cdot T_a + h_{pf} \cdot T_f}{U_{L2} + h_{pf}} \tag{4}$$

where $(\alpha\tau)_{2,eff}$ is the product of effective absorptivity of absorber plate and transmittivity of the covered glass, PF_1 is the penalty factor [39] due to the glass cover of module, and U_{L2} is the overall heat transfer coefficient from the plate to ambient.

The energy balance of the fluid (water) flowing in the pipes under the absorber plate is as follows:

$$\dot{m}_f \cdot c_f \frac{dT_f}{dx} = b \cdot F' \cdot [DNI \cdot PF_2 \cdot (\alpha\tau)_{m,eff} - U_{l,m} \cdot (T_f - T_a)]dx \tag{5}$$

where $\dot{m}_f$ is the mass flow rate of fluid water, 0.02 kg/s [36], c_f is the specific heat of water, $(\alpha\tau)_{m,eff}$ is the product of the effective absorptivity of the absorber plate and the mixed transmittivity of the PV module and covered glass, b is the width of the receiver, PF_2 is the penalty factor due to plate below the module, and $U_{l,m}$ is the overall heat transfer coefficient from the module to the ambient.

The outlet temperature of the fluid at the end of PV module, T_{fom} is [39]:

$$T_{fom} = [\frac{PF_2 \cdot (\alpha\tau)_{m,eff}}{U_{l,m}} + T_a] \cdot [1 - \exp\{\frac{-F^{'} \cdot U_{l,m} \cdot A_{rm}}{\dot{m}_f \cdot c_f}\}] + T_{fi} \cdot \exp(\frac{-F^{'} \cdot U_{l,m} \cdot A_{rm}}{\dot{m}_f \cdot c_f}) \quad (6)$$

where T_{fi} is the inlet temperature of water (80°C) [30].

The outlet temperature (T_{fo}) of the CPC-PVT is calculated as [39]:

$$T_{fo} = [\frac{PF_c \cdot (\alpha\tau)_{c,eff} \cdot DNI}{U_{L,c}} + T_a] \cdot [1 - \exp\{\frac{-F^{'} \cdot U_{L,c} \cdot b}{\dot{m}_f \cdot c_f}\}] + T_{fi} \cdot \exp\{\frac{-F^{'} \cdot U_{L,c} \cdot b}{\dot{m}_f \cdot c_f}\} \quad (7)$$

where PF_c is the penalty factor due to the glass cover for the portion covered by glazing.

The electrical efficiency (η_m) of PV cell is affected by the PV module temperature and it can be determined by the following equation [36]:

$$\eta_m = \eta_0 \cdot [1 - \chi \cdot (T_{cell} - T_0)] \quad (8)$$

where η_0 and η_{cell} are the electrical efficiencies in standard and actual conditions, respectively. χ is the temperature coefficient of the PV efficiency [36].

The solar electricity output from the PV/T ($E_{PV/T}$) is defined as:

$$E_{PV/T} = DNI \cdot A_{PV} \cdot \eta_m \cdot 10^{-3} \quad (9)$$

where A_{PV} is the area of the PV cell.

The thermal energy ($Q_{en,sol}$) from the collector is related to the inlet and outlet temperatures, and mass flow rate of the fluid:

$$Q_{en,PV/T} = \dot{m}_f \cdot c_f \cdot (T_{fo} - T_{fi}) \quad (10)$$

The energy and exergy efficiency were chosen for the performance evaluation of the PV/T based on the first and second law of thermodynamics:

$$\eta_{en,PV/T} = \frac{Q_{en,PV/T} + E_{PV/T}}{Q_{en,sol}} \times 100\% \quad (11)$$

$$\eta_{ex,PV/T} = \frac{Q_{ex,PV/T} + E_{PV/T}}{Q_{ex,sol}} \times 100\% \tag{12}$$

where $\eta_{en,PV/T}$, $\eta_{ex,PV/T}$ are the energy and exergy efficiencies of the PV/T unit, respectively.

2.3.2 Absorption heat pump

The single effect AHP is used to absorb heat from the solar thermal (state 4) and geothermal water circuit (state 19) to produce space heating water (state 9) by heating the returned water (state 13). The strong solution (state a8) and steam (state a1) in the AHP is generated in the generator by absorbing heat from the solar heating fluid. The steam is utilized to heat the space heating water in the condenser and then it is fed to the evaporator to absorb heat from geothermal water. Water and the strong solution are mixed with an exothermic reaction and the resulting reaction heat is used to preheat the space heating water [34]. The flowchart of the AHP is described in detail in Fig. 4.

The mathematical equations describing the key components of the AHP are given in Table 1.

Table 1. Mathematical equations for modelling the AHP [34].

Component	Equation
Generator	$Q_g = \dot{m}_{a8} \cdot h_{a8} - \dot{m}_{a7} \cdot h_{a7} + \dot{m}_{a1} \cdot h_{a1}$; $\dot{m}_{a8} = \dot{m}_{a7} - \dot{m}_{a1}$; $\dot{m}_{a8} \cdot \varsigma_{a8} = \dot{m}_{a7} \cdot \varsigma_{a7}$ $Q_g = U_g \cdot A_g \cdot LMTD_g$
Condenser	$Q_{co}^{AHP} = \dot{m}_{a1} \cdot (h_{a1} - h_{a2})$; $Q_{co}^{AHP} = U_{co}^{AHP} \cdot A_{co}^{AHP} \cdot LMTD_{co}^{AHP}$
Evaporator	$Q_{eva}^{AHP} = \dot{m}_{a3} \cdot h_{a3} - \dot{m}_{a2} \cdot h_{a2} = c_{16} \cdot \dot{m}_{16} \cdot (T_{18} - T_{16})$; $Q_{eva}^{AHP} = U_{eva}^{AHP} \cdot A_{eva}^{AHP} \cdot LMTD_{eva}^{AHP}$
Absorber	$Q_{ab} = \dot{m}_{a3} \cdot h_{a3} + \dot{m}_{a9} \cdot h_{a9} - \dot{m}_{a5} \cdot h_{a5}$; $\dot{m}_{a5} = \dot{m}_{a3} + \dot{m}_{a9}$ $\dot{m}_{a9} \cdot \varsigma_{a9} = \dot{m}_{a5} \cdot \varsigma_{a5}$
	$Q_{ab} = U_{ab} \cdot A_{ab} \cdot LMTD_{ab}$
Heat exchanger	$\eta_{HX} \cdot \dot{m}_{a8} \cdot (h_{a8} - h_{a9}) = \dot{m}_{a5} \cdot (h_{a6} - h_{a5'})$; $Q_{HX} = U_{HX} \cdot A_{HX} \cdot LMTD_{HX}$
Space heating	$Q_{heat}^{AHP} = Q_{ab} + Q_c^{AHP}$

Table 1 symbols are explained in the following: h, ς are the enthalpy and concentration of each state, respectively. U_i, A_i and $LTMD_i$ are the heat transfer coefficient, heat transfer area and logarithmic mean temperature difference for the i^{th} component, respectively. The temperatures of ground source water are set at 37°C (T_{18}), and 19°C (T_{16}) [30]. The subscripts *co*, *eva*, *ab*, *HX*, *g* represent the condenser, evaporator, absorber, heat exchanger, and generator, respectively. The subscript numbers are seen in Fig. 4.

The coefficient of performance (COP_{AHP}) describes the performance of the AHP:

$$COP_{AHP} = \frac{Q_{heat}^{AHP}}{Q_{4/5} + Q_{6/7}} \tag{13}$$

where Q_{heat}^{AHP} is the space heating output.

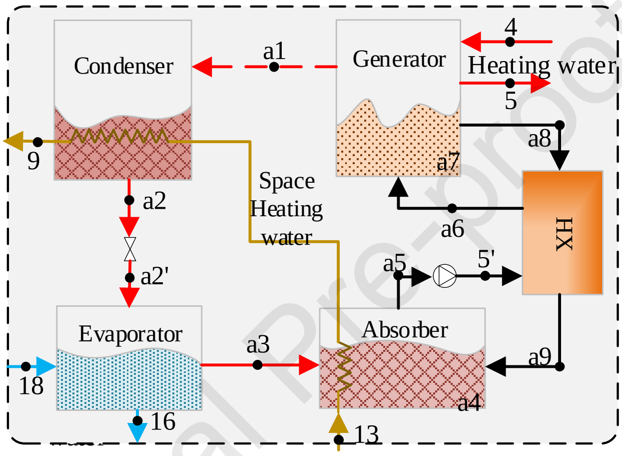

Fig. 4. Energy flowchart of the single-effect absorption heat pump.

2.3.3 Geothermal heat pump

The geothermal heat pump (GSHP) provides space heating at high heating load conditions. The GSHP is driven by solar or off-grid electricity.

Based on [35], the main equations for describing the GSHP are given in Table 2.

Table 2. Mathematical equations for modelling the GSHP [35].

Component	Equations
Compressor	$E_{com} = (\frac{n}{n-1} \cdot \dot{m}_{com} \cdot R \cdot (T_{co}^{GSHP} - T_{eva}^{GSHP})) / \eta_{com}$
	$T_{eva}^{GSHP} = (T_{19} \cdot e^{(\eta_{eva}^{GSHP} \cdot A_{eva}^{GSHP})/(m_{15} \cdot c_{15})} - T_{15}) / (e^{(\eta_{eva}^{GSHP} \cdot A_{eva}^{GSHP})/(m_{15} \cdot c_{15})} - 1)$
	$T_{co}^{GSHP} = (T_{12} \cdot e^{(\eta_{co}^{GSHP} \cdot A_{co}^{GSHP})/(m_{12} \cdot c_{12})} - T_{10}) / (e^{(\eta_{co}^{GSHP} \cdot A_{co}^{GSHP})/(m_{12} \cdot c_{12})} - 1)$
Throttle valve	$h_{in}^{th} = h_{out}^{th}$; $\dot{m}_{in}^{th} = \dot{m}_{out}^{th}$

Condenser	$Q_{co}^{GSHP} = Q_{heat}^{GSHP} = c_{10} \cdot \dot{m}_{10} \cdot (T_{10} - T_{12})$
Evaporator	$Q_{eva}^{GSHP} = c_{19} \cdot \dot{m}_{19} \cdot (T_{19} - T_{15})$

where *n*, and *R* are the variable coefficient and the ideal gas constant. η_{com}, η_{eva}^{GSHP}, and η_{co}^{GSHP} are the electrical efficiency of compressor, and heat transfer efficiencies of the evaporator and condenser, respectively. The subscripts *th* and *com* stands for the throttle valve and compressor.

The COP of the GSHP is given by:

$$COP_{GSHP} = \frac{Q_{heat}^{GSHP}}{E_{com}} \tag{14}$$

2.3.4 Thermal energy storage

The solar thermal output (outlet temperature is set to 80°C) from the PV/T-unit is utilized to preheat the water (heat transfer fluid) in the TES tank. The TES model is simplified by assuming a well-mixed water tank, i.e. no thermal stratification of water. Other assumptions are based on [40]. The mathematical model of the water tank is based on [40, 41].

The energy balance of the tank can be described as:

$$(\rho V C_p)\frac{dT_{TES}}{dt} = Q_{in} - Q_{out} - (UA)_{TES}(T_{TES} - T_a) \tag{15}$$

where ρ stands for density, V is the volume of thermal tank, C_p is the specific heat of water, T_{TES} is the average temperature in the thermal tank, t is the time, Q_{in} and Q_{out} are the solar thermal input and discharged heat, respectively. U and A_{TES} are heat transfer coefficient and heat transfer area of the thermal tank.

The discharged energy from the thermal tank can be calculated as:

$$Q_{ou} = m_{6-7} C_p (T_{TES} - T_{in}) \tag{16}$$

The energy efficiency of the thermal tank (η_{TES}) is expressed as [42]:

$$\eta_{TES} = \frac{Q_{out}}{Q_{in}} \times 100 \tag{17}$$

2.3.5 Validation of the models

The following validation procedure was adopted [43]:

(1) In the PV/T-unit, the PV module temperature calculated by Eq. (2) is compared with [44] under the same environmental conditions in (Fig. 5a) [44], and the mass flow rate is 0.012 kg/s. The RMSE between the two models is 6.6% on average, which shows a satisfactory accuracy of the present model;

(2) The capacity of each component of the AHP calculated with the equations in Table 1 are compared with [34] in Table 3. The external flows including the geothermal water, space heating water, and space heating water are the same as in [34]. The results in Table 3 indicate relative errors less than 5%;

(3) The COP of the GSHP is compared to [45] in Fig. 5(b) for different preheating temperatures. Increasing the ground water temperature (T_{19} in Table 2) corresponds to a higher energy performance. The RMSE of the comparison is 4.6%, which is for the thermodynamic analysis;

(4) The thermal tank energy efficiency is set to 80% [42].

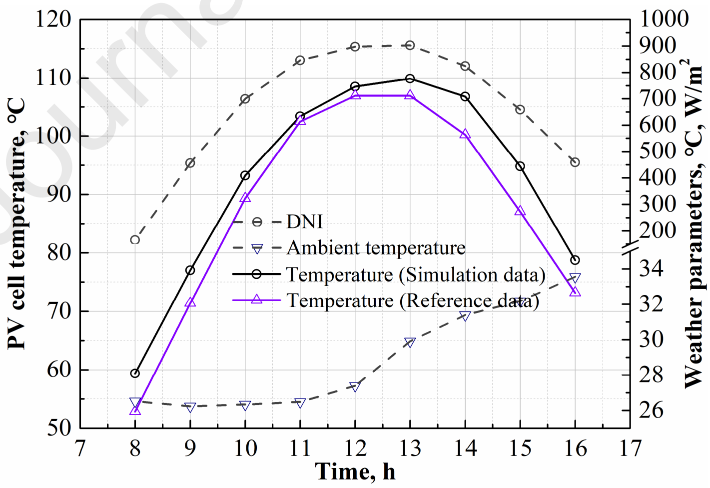

(a)

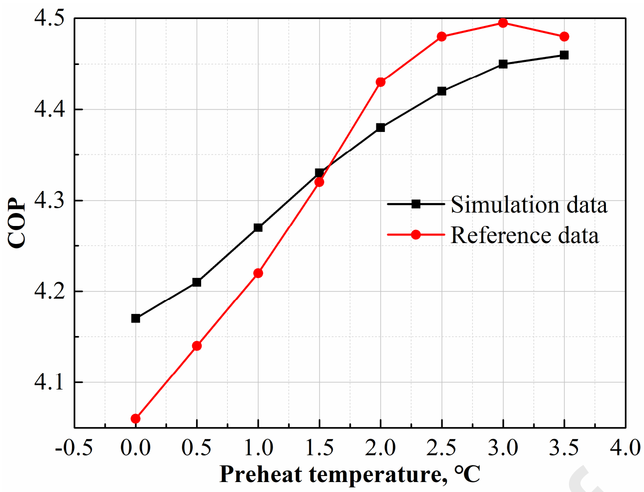

(b)

Fig. 5 Comparision between reference data and this study: (a) PV/T, (b) GSHP.

Table 3. Comparison of thermal power levels of AHP components.

	Simulation data, kW	Reference data, kW [34]
Generator	2893	2893
Absorber	2741	2769
Evaporator	2317	2250
Condenser	2469	2373

3. Assessment and optimization method

3.1 Assessment criteria

In the following, the assessment criteria used are presented.

3.1.1 Energy and exergy efficiencies

(1) Energy efficiency [46]:

$$\eta_{en,sys} = \frac{\sum_{r=1}^{8760} (Q_{heat}^{AHP,r} + Q_{heat}^{GSHP,r})}{\sum_{r=1}^{8760} Q_{pri}^{r}} \times 100\% \quad (18)$$

(2) Exergy efficiency [46]:

$$\eta_{ex,sys} = \frac{\sum_{r=0}^{8760} (Ex_{heat}^{AHP,r} + Ex_{heat}^{GSHP,r})}{\sum_{r=0}^{8760} Ex_{pri}^{r}} \times 100\% \quad (19)$$

where Q_{pri}, and Ex_{pri} are the primary energy and exergy consumption, respectively. r is the r^{th}

hour of the year.

3.1.2 Modified thermo-ecological cost

The thermo-ecological cost (TEC) method [21, 22] is based on exergy analysis and is able to assess the cumulative exergy consumption of specific products. TEC is modified here through the following assumptions [27]: (1) The impacts of byproducts are ignored; (2) The import construction materials are ignored; (3) The products are utilized locally.

The balance equation for the TEC analysis is defined as follows [27]:

$$TEC_j = \sum_s b_{sj} + \sum_i a_{ij} TEC_i + \sum_k p_{kj} \xi_k \tag{20}$$

where TEC_j is the CExC of the product of j^{th} process, $\sum_i b_{sj}$ is the cumulative exergy consumption of non-renewable resources, s is the s^{th} non-renewable resource. $\sum_i a_{ij} TEC_i$ is the cumulative exergy consumption of the i^{th} process. $\sum_k p_{kj} \xi_k$ is the cumulative exergy consumption of the environmental losses caused by the harmful substances. p and ξ are the pollutant emissions and compensation cost, k is the k^{th} pollutant. The compensation costs for the emissions are given in Table 4.

Table 4. Compensation cost of pollutant emissions [47].

Compensation cost	Value, kWh/kg
SO_x	27.17
NO_x	19.97
PM	14.84

The energy consumption b_{sj} and pollutant emissions p_{sj} during the initial construction and operation processes are given by:

$$b_{sj} = \dot{b}_{sj}^{ini} + b_{sj}^{ope} \tag{21}$$

$$p_{sj} = \dot{p}_{sj}^{ini} + p_{sj}^{opera} \tag{22}$$

where $\dot{b}_{sj}^{ini}$ and b_{sj}^{ope} are the hourly non-renewable resource consumptions during the initial construction and operating stages. $\dot{p}_{sj}^{ini}$ and p_{sj}^{opera} are the hourly pollutant emissions during the initial construction and operating stages:

$$\dot{b}_{sj}^{ini} = b_{sj}^{ini} / L \tag{23}$$

$$\dot{p}_{sj}^{ini} = p_{sj}^{ini} / L \tag{24}$$

where b_{sj}^{ini} and p_{sj}^{ini} are the yearly non-renewable resource consumptions and pollutant emissions during the initial construction stage. L stands for the yearly operating hours. The energy input and material consumption of each component during the initial construction stage are given in Tables 5 and 6.

Table 5. Pollutant emissions and electricity consumption of raw materials [48, 49].

Parameters		Material				
		Steel	Aluminum	Copper	PVC	Glass
Pollutant Emissions, g/kg	SO_x	9.7	205.5	17.7	3.4	1.1
	NO_x	4.0	94.7	11.5	2.8	3.7
	PM	15.0	290.0	-	2.2	7.0
Electricity, kWh/kg		1.7	36.1	1.8	21.9	0.6

Table 6. Material and electricity consumption of system components [48-50].

Parameters	Solar collector	PV module	AHP	GSHP	TES
Steel, kg/kW	2.5	27.0	18.4	12.9	1.0
Aluminum, kg/kW	1.1	10.5	-	4.7	-
Copper, kg/kW	-	-	-	3.9	-
PVC, kg/kW	4.7	9.2	-	-	-
Glass, kg/kW	0.8	80.0	-	-	-
Electricity, kWh/kW	5.9	82.0	11.9	14.0	1.0

Based on the TEC analysis mentioned above, the unit thermo-ecological cost (UTEC) can be determined as the ratio of the cumulative exergy consumption (TEC_j) to the product exergy (Ex_j):

$$UTEC_j = \frac{TEC_j}{Ex_j} \tag{25}$$

However, for the multi-products devices such as the PV/T-unit, the *UTEC* of the solar hot water and solar electricity are same, and thus the energy levels between the two products are ignored in the conventional TEC method [27]. In this study, the energy level (*EL*) of the product is considered through the following equation [51]:

$$EL = \frac{\Delta Ex}{\Delta H} = 1 - T_0 \frac{\Delta S}{\Delta H} \tag{26}$$

where ΔEx, ΔH, and ΔS are the exergy, enthalpy, and entropy changes, respectively.

For each unit in Fig. 2, the TEC is calculated as follows:

CPC-PV/T:

$$TEC_{2-5} + TEC_1 = b_{PV/T} + UTEC_0 Ex_0 + \sum_k (p_k \xi_k)_{PV/T} \tag{27}$$

$$\frac{TEC_{2-5} Ex_1}{TEC_1 Ex_{2-5}} = \frac{EL_{2-5}}{EL_1} \tag{28}$$

where $UTEC_0$, is the unit TEC of solar irradiance, 0.02 J/J [52]. The subscript numbers refer to the states in the flowchart in Fig. 2.

AHP:

$$TEC_{9-13} = b_{AHP} + TEC_{4-5} + TEC_{6-7} + \sum_k (p_k \xi_k)_{AHP} \tag{29}$$

TES:

$$TEC_{6-7} = b_{TES} + TEC_{3-5} + \sum_k (p_k \xi_k)_{TES} \tag{30}$$

GSHP:

$$TEC_{10-12} = b_{GSHP} + TEC_1 + TEC_{14} + \sum_k (p_k \xi_k)_{GSHP} \tag{31}$$

It should be noted that due to the lower energy level of ground water, the TEC of the ground water is ignored.

Finally, the UTEC of space heating water ($UTEC_{8-11}$) can be determined as follows:

$$UTEC_{8-11} = \frac{TEC_{9-13} + TEC_{10-12}}{Ex_{9-13} + Ex_{10-12}} \tag{32}$$

3.2 Optimization method

The TES-unit can adjust the space heating output by absorbing solar thermal energy or discharging heat to the AHP. The capacity of the TES also influences the *UTEC* of the space heating water. In this study, the heat storage ratio (ε_{TES}) is used to describe the impacts of the TES. ε_{TES} is expressed as the ratio of the stored heat in the TES to the output heat from the CPC-PV/T:

$$\varepsilon_{TES} = \frac{\sum_{r=1}^{8760} Q_{TES}^{r}}{\sum_{r=1}^{8760} Q_{PV/T}^{r}} \tag{33}$$

In the analysis of the proposed system, the PV coverage area is used as a variable parameter to adjust the solar thermal and electricity output. When the PV module area is 0, the PV/T subsystem has no solar electricity output, while the fluid circulation in the PV/T can only absorb heat from the PV module when the PV/T is fully covered by PV module. The PV coverage ratio ($\varepsilon_{PV} \subset [0,1]$) defined as the PV area to the total PV/T area is selected as a decision variable:

$$\varepsilon_{PV} = \frac{A_{PV}}{A_{PV/T}} \tag{34}$$

Based on the modified TEC analysis in Sec. 3.1.2, the unit thermo-ecological cost of space heating water is determined as the objective function, which is set as min [$UTEC_{8\text{-}11}$].

The modified TEC optimization procedure is shown in Fig. 6. The environmental, building load, and technical informations are initialized as input parameters. The thermodynamic and thermal models of each unit are constructed next. Based on the initial parameters and models, the modified TEC analysis is then performed. The optimization against the decision variable is continued until satisfies convergence. The quadratic approximation algorithm [53] in the EES software is selected as the optimization algorithm for the hybrid heating system with a convergence tolerance of 10^{-4}.

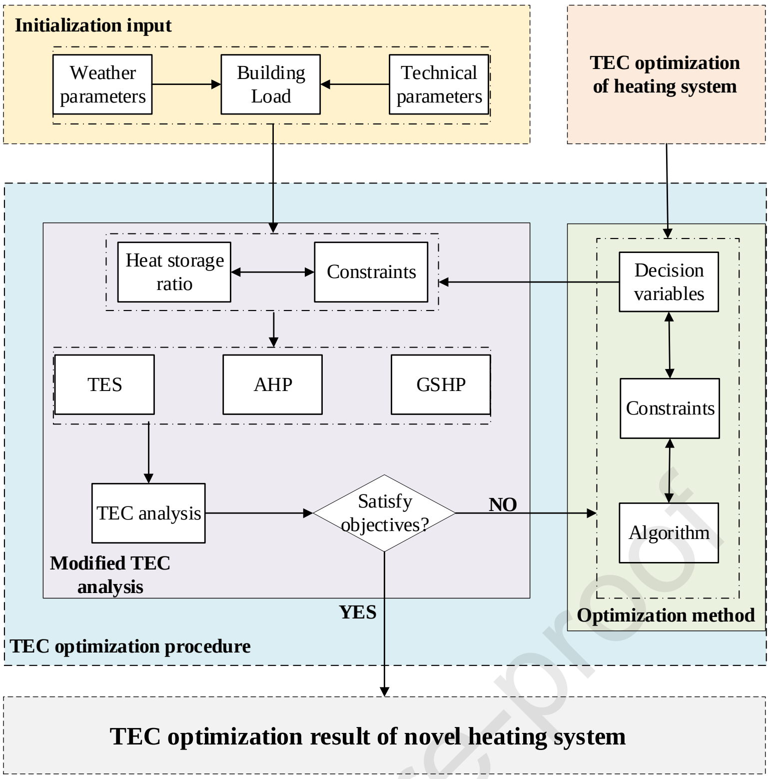

Fig. 6. Optimization procedure of proposed heating system.

4. Results

The thermal performance analysis and the modified TEC optimization is presented in the next. Before the simulation, the solar collector area was fixed based on the shading and maintenance area needed. The available area for the CPC-PV/T is almost 60% [36] of the total roof area, corresponding to max. 168 sets of PV/T-units (two units are connected in series and 84 units are installed in parallel).

4.1 Effect of ambient conditions on performance

The performance of the CPC-PV/T affected by the ambient and technical parameters has a strong influence on the overall performance of the proposed system. To evaluate the performance at variable conditions, it is assumed that: (1) The solar thermal energy and solar electricity are fed to the AHP and GSHP to generate space heating energy; (2) The contributions of the TES and the grid electricity are ignored; (3) The ambient temperature is set to 25° C. The performance as function of the direct normal irradiance and the PV-coverage ratio is discussed next.

4.1.1 Performance versus direct normal irradiance

The PV-coverage ratio is set here to 0.5, i.e., 50% of the PV/T area is covered by PV modules.

Fig. 7(a) shows the performance of the CPC-PV/T with different DNI values. The critical DNI value under which the thermal collector is not able to deliver heat is 325W/m^2.This is higher than the 286 W/m^2 reported in [36]. Increasing the DNI from 325 W/m^2 to 1000 W/m^2, the solar thermal output is increased linearly from 3kW to 124kW, while the and the solar electricity raises 130.27%. However, due to the lower energy level (Eq. 25), the solar thermal exergy is less than 1/5 of the thermal energy output.

Observing the energy and exergy efficiencies in Fig. 7(a), both curves show a similar trend: the efficiencies improve quickly at first with increasing DNI, and then raise up to the maximum values (48.78% and 15.30%) with a decreasing rate. Over the whole range of DNI values considered, the energy and exergy efficiencies raise 347.52% and 64.69%, respectively. Compared to [36] with a 70°C fluid inlet temperature, the solar device in this study reaches a lower energy efficiency, but a higher exergy performance, with the same DNI. The reason is that with a higher inlet temperature the solar thermal energy output decreases, but it has a positive impact on the exergy output.

The performance of the whole heating system is shown in Fig. 7(b). The COP of the AHP behaves similarly than the energy efficiency in Fig. 7(a). The COP increases on average by 0.04 units for each 25 W/m^2 of DNI increase, because of the higher fluid output temperature from the solar thermal unit. The energy and exergy efficiencies decrease 132.67% and 135.09%, when the DNI decreases from 1000 W/m^2 to 325 W/m^2. The exergy efficiency of the hybrid system is < 6% due to the lower energy level of space heating water.

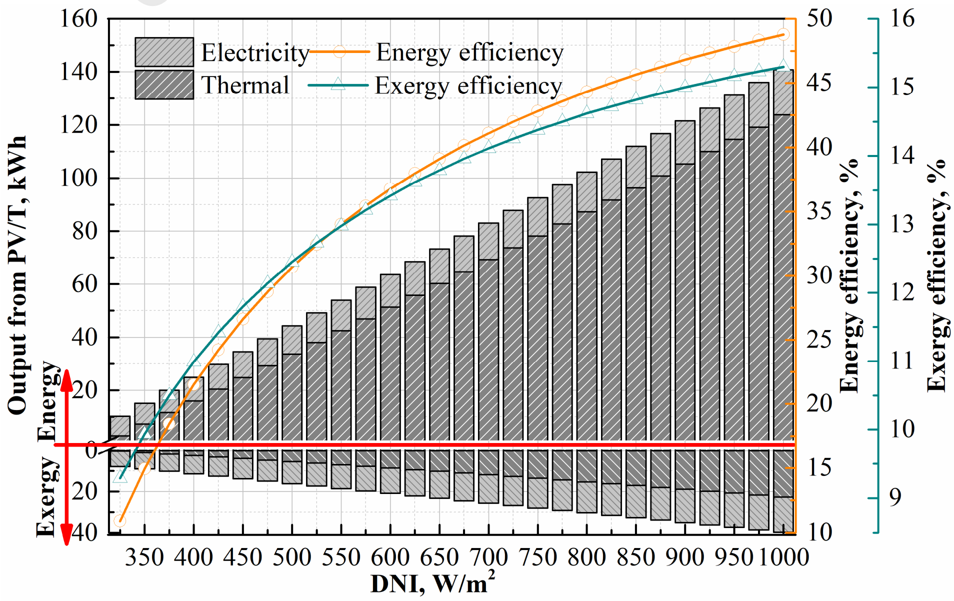

(a)

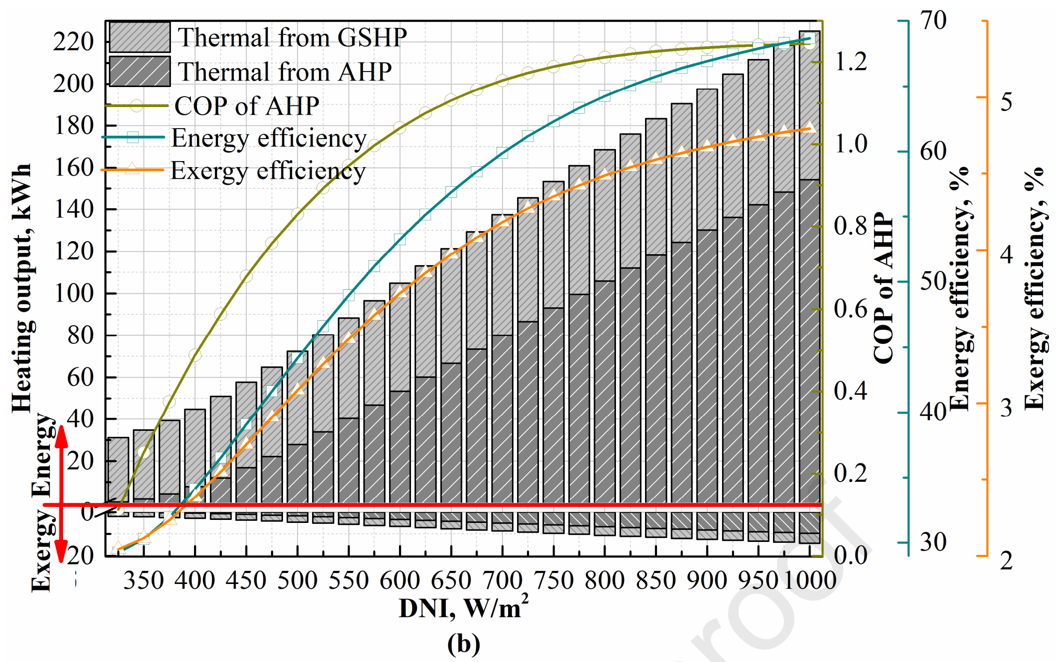

Fig. 7. Performance versus direct normal irradiance (DNI). (a) Performance of the CPC-PV/T, (b) Performance of the AHP and the hybrid system.

4.1.2 Performance versus PV-coverage ratio

To search the impacts of PV coverage ratio, the DNI in this section is determined at 800 W/m^2. The PV coverage ratio is varied in the range [0, 1.0]. The simulated results are displayed in Fig. 8.

Differently to the increasing energy output in Fig. 7(a), the energy output is decreased steeply as the ε_{PV} raises, although the electricity output increases from 0 kW to 30.1 kWh. However, the total exergy output is obviously increased from 19.8 kWh to 41.0 kWh, causes by the higher incresing solar electricity and lower decreasing solar thermal exergy. As a result, the energy and exergy efficiencies trend opposite: The energy efficiency decreases 13.83%, while the exergy efficiency raises 107.18%, with the whole considered range of ε_{PV}.

In Fig. 8(b), the COP of AHP decreases by 0.011, when the ε_{PV} increases 0.1. The reason is that the ε_{PV} decreases the outlet temperature of solar hot water, which results a lower COP of AHP. Based on the decreasing COP and thermal energy from PV/T, the space heating output from AHP drops linearly as Fig. 8(b) shows. On the other hand, the heating energy output from GSHP dramatically raises from 0 kWh to 125.4 kWh. Due to the higher COP of GSHP, the energy efficiency of hybrid system increases with improving ε_{PV}, although the heating energy from AHP declines. The ε_{PV} also has the positive impact on the exergy efficiency, and when ε_{PV} changes 0.1, the exergy efficiency increases by 0.17.

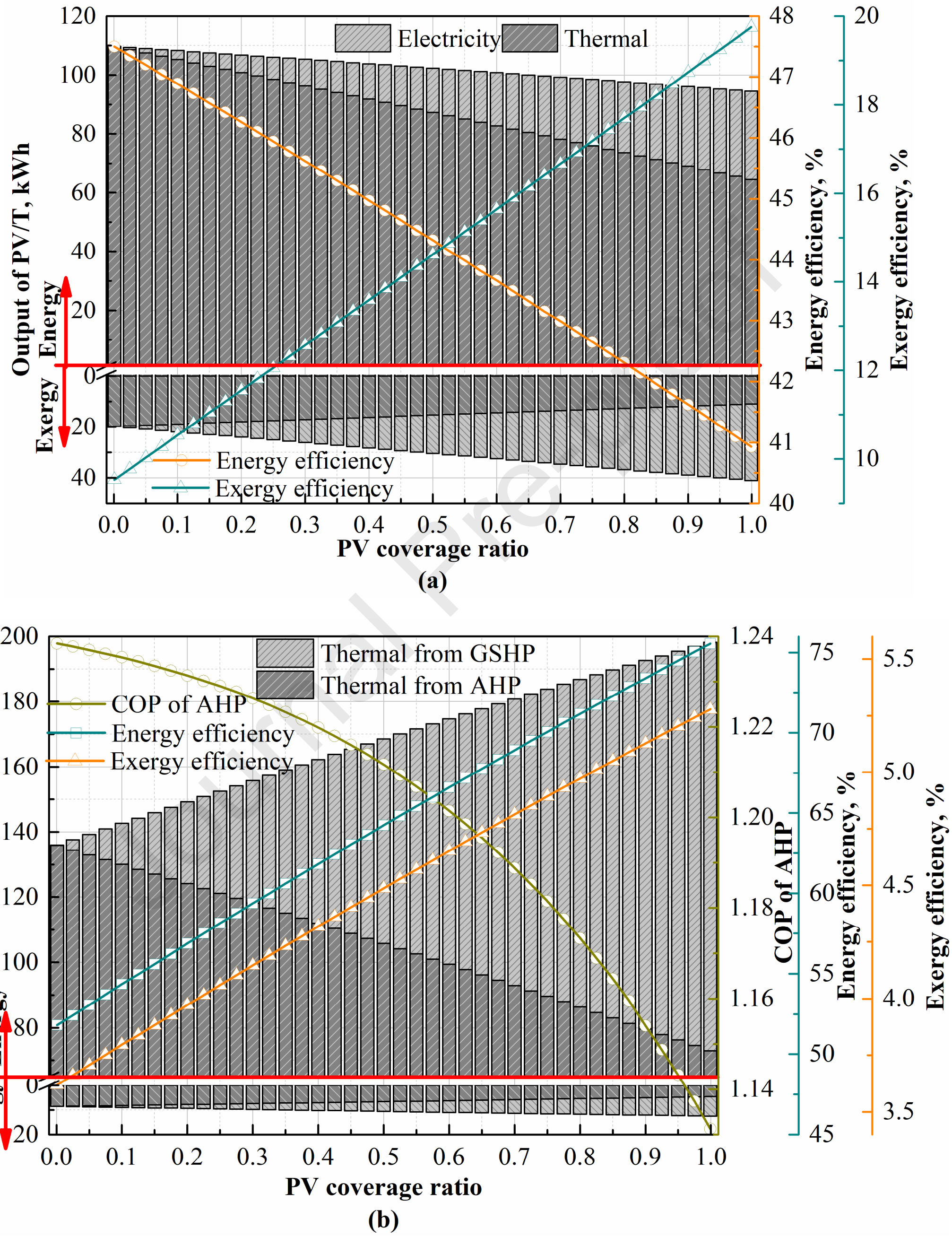

Fig. 8. Performance as a function of the variable PV coverage ratio (ε_{PV}): (a) Performance of the CPC-PV/T, (b) Performance of the AHP and heating system.

4.2 Modified TEC optimization

The yearly environmental parameters and building loads are transformed to a design condition based on the method in [51]. The details are concluded as follows:

(1) The total DNI for the whole year is 1.4 MW/m^2, and the DNI in design condition is set at 800 W/m^2, the annual operation time of CPC-PV/T is 1746 hours. The yearly average ambient temperature is 12.6° C.

(2) An increasing ε_{PV} corresponds to an improving wasted solar electricity. The solar electricity ratio, $\varepsilon_{PV/T}^{use}$, is defined as the ratio of the utilized solar electricity to the total solar electricity, is used to evaluate the useful solar electricity, and it can be determined by the fitting formula in [30] ($\varepsilon_{PV/T}^{use} = -0.43\varepsilon_{PV} + 1$).

(3) The nominal capacity of the GSHP is equal to the maximal heating load (300 kW).

(4) The yearly space heating demand is 454 MWh. During the optimization, the heating load is first covered by the CPC-PV/T unit and the possible shortage in heat is then met by the GSHP worked with full load.

(5) The heat storage ratio ($\varepsilon_{TES} \in [0.1,1]$) is set to 0.1 during the optimization process.

4.2.1 Optimization results

Using the 'quadratic approximations' method in EES software [38], the optimization result is displayed in Table 7. The optimal PV coverage ratio with modified TEC method is found at 0.66. In this condition, the optimized unit thermo-ecological cost of space heating water is 6.86 J/J. The UTEC of space heating water from GSHP is 9.92 J/J, and it is almost 50 times higher than the cost from AHP. Compared to the conventional method, the heating cost of system is lower by 0.03 J/J. To validate the result, the variation of UTEC as a function of PV coverage ratio (ε_{PV}) is dispalyed in Fig. 9.

It can be found in Fig. 9 that as the ε_{PV} increases, the UTEC of space heating water decreases quickly to a minimum value, and then as the ε_{PV} increases from the critical point (0.66) to 1, the UTEC increases steeply.

Table 7. Optimization results based on two TEC methods.

Parameters	Modified TEC method, J/J	Conventional TEC method [27], J/J
PV coverage ratio	0.66	0.66
$UTEC_{8\text{-}11}$ (hybrid system)	6.86	6.91
$UTEC_{9\text{-}13}$ (AHP)	0.20	0.67
$UTEC_{10\text{-}12}$ (GSHP)	9.92	9.79

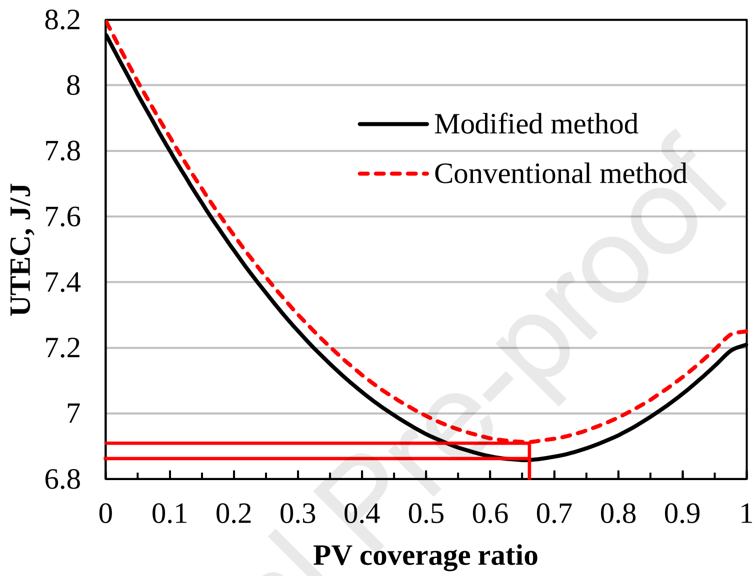

Fig. 9. UTEC versus PV-coverage ration with the modified and conventional TEC-method.

4.2.2 Sensitivity analysis

The optimization results are affected by the choice of the initial parameters such as operating hours of the PV/T-unit, TEC-cost of solar irradiance and grid electricity, among others. Therefore, a sensitivity analysis against these parameters is highly relevant and is presented in the next.

(1) PV-coverage ratio

ε_{PV} influences the UTEC of the solar hot water and solar electricity, which in turn affects the TEC of the hybrid system. The UTECs of subsystems are shown in Fig. 10. Fig. 10(a) shows that the modified UTEC of the solar water and solar electricity and the UTEC of the PV/T analyzed with the conventional method steeply decrease with increasing PV-coverage ratio. When ε_{PV} increases from 0 to 0.3, the modified cost of the solar electricity and solar hot water decrease by 70.19%, and 70.64%, respectively, while the drop is 17.87% only when calculated with the conventional method. When ε_{PV} increases from 0.3 to 1, the UTEC of solar electricity and solar water decrease by 0.33

J/J and 0.06 J/J, respectively. The modified UTEC of solar electricity is higher than that of the conventional UTEC of the PV/T, while the modified solar hot water cost is lower due to the lower energy level of hot water.

The space heating water costs of GSHP and AHP are shown in Fig. 10(b). Compared to the conventional cost, the modified cost of hot water from the GSHP is higher for the whole range of ε_{PV}, while the cost of the AHP output has a similar trend than the modified cost of solar hot water in Fig. 10(a). During the operation of the system, the GSHP consumes solar electricity, while the AHP absorbs solar heat, which has a lower UTEC.

On the other hand, the difference of the UTEC of the GSHP calculated with the modified and conventional methods is smaller than the corresponding difference of the AHP. The reason for this is that the GSHP also uses grid electricity as the solar electricity contributes much less to the GSHP electricity, although the UTEC of solar electricity is lower. The fuel in the AHP is solar heat only. The space heating water cost from the GSHP is on average 36 times higher than that of the AHP.

When ε_{PV} > 0.66, the UTEC of space heating water from the PV/T and GSHP decreases slowly. In this region, the AHP produce less space heating, while the output from the GSHP increases. Moreover, the surplus of solar electricity increases with increasing ε_{PV} due to supply and demand mismatch. Thus, when ε_{PV} > 0.66, the UTEC of space heating water for the whole hybrid system is closer to the cost of space heating water from GSHP.

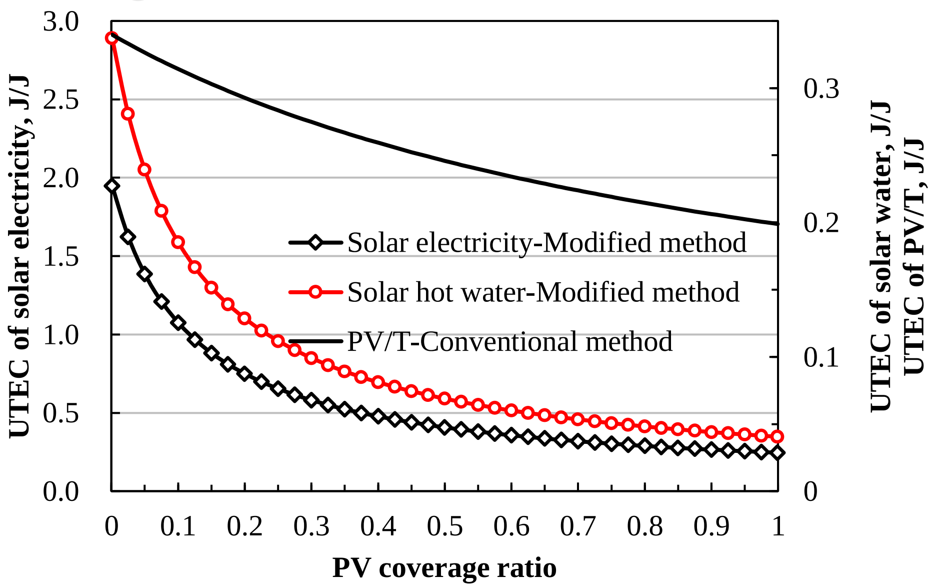

(a)

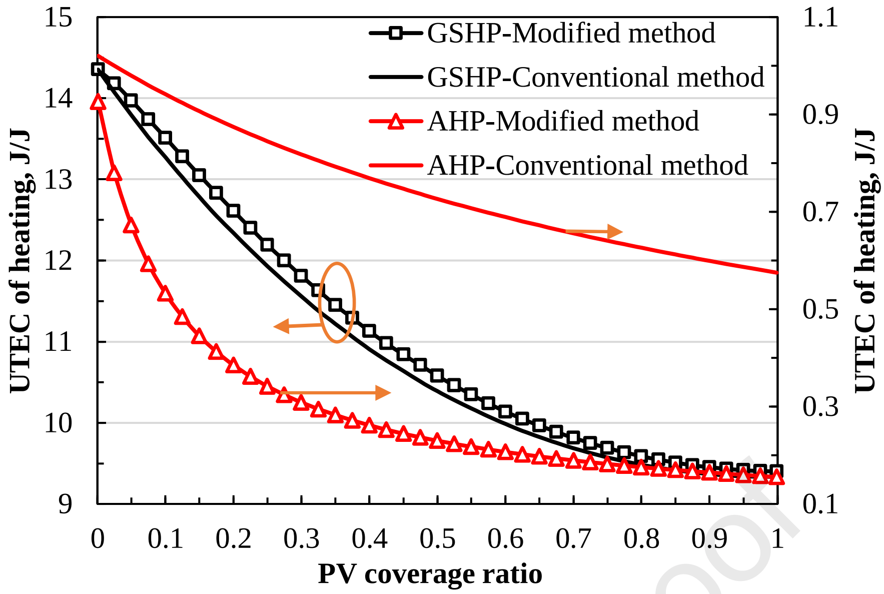

(b)

Fig. 10. Change in the UTEC of the subsystems with PV-coverage ratio with the modified and conventional TEC-method.

(2) Operating hours

The operating hours are analyzed with an average solar radiation level of 800W/m^2, and the variation in the yearly solar irradiance is accounted by varying the operating hours of the CPC-PV/T. Here, a range of 1000-3000 hours is used.

Fig. 11 shows the UTECs when varying the number of operating hours in a year. In Fig. 11(a), the solar UTECs which steeply decrease over the whole range. Increasing the operating hours by 1000 hours, decreases the UTEC costs of solar electricity and solar hot water by 14.33%, and 14.42%, respectively. As a result of decreasing cost of solar hot water, the cost of outlet water from the TES decreases by 29.91% for the whole range of operating time (1000 – 3000 hours).

The costs of space heating water of the hybrid system (GSHP and AHP) are shown in Fig. 11(b). Based on the decreasing cost of solar hot water and solar electricity, the UTECs of space heating water from the AHP and GSHP decrease over the whole range by 0.12 J/J and 8.83 J/J, respectively. This result has also affected to the decreasing trend of space heating cost for the hybrid system which decreases from 9.99 J/J to 1.59 J/J over the whole range.

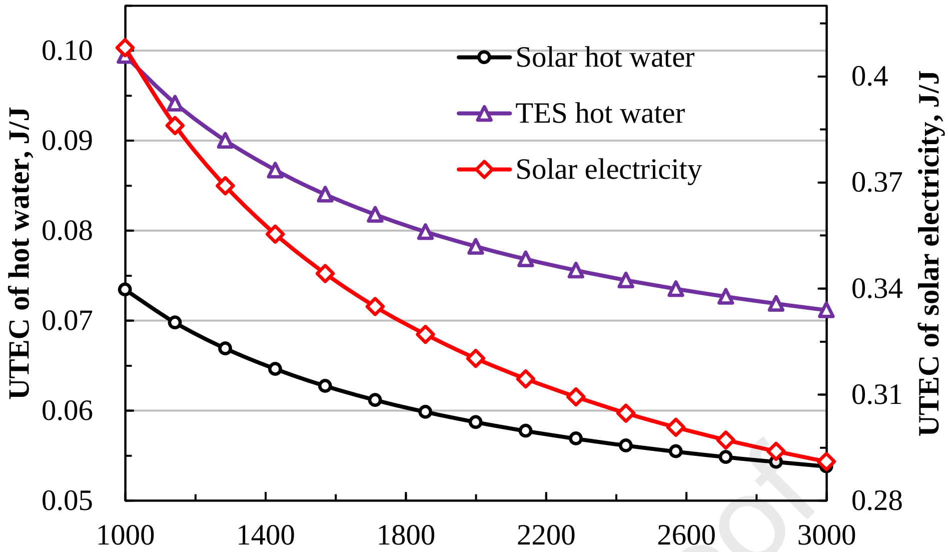

(a)

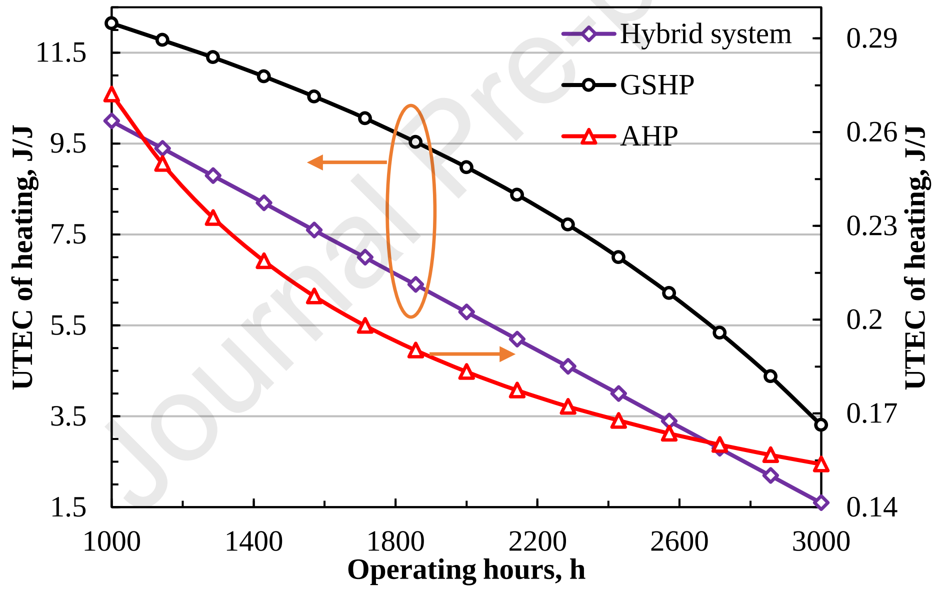

(b)

Fig. 11. Change in UTEC of the subsystems as a function of the operating hours using the modified TEC-method.

(3) UTEC of solar irradiance and grid electricity

The UTEC of the solar irradiance and grid electricity are determined based on the reference data. These have a higher impact on the UTEC of the GSHP, because the GSHP consumes both solar and grid electricity. Fig. 12 shows that the UTEC of the space heating water from the GSHP and the hybrid system increases with increasing UTEC of grid electricity. For each increase of 0.1 J/J of grid electricity, the costs of GSHP and hybrid system increase by 0.27 J/J and 0.18 J/J, respectively. On the other hand, when the cost of irradiance increases by 0.01 J/J, the cost of GSHP and the hybrid system increase by 0.15 J/J and 0.12 J/J, respectively. For the whole range considered, the lowest UTEC of space heating is 8.34 J/J (GSHP) and 5.76 J/J (system), while the maximum UTEC is 12.22 J/J and 8.54 J/J, respectively.

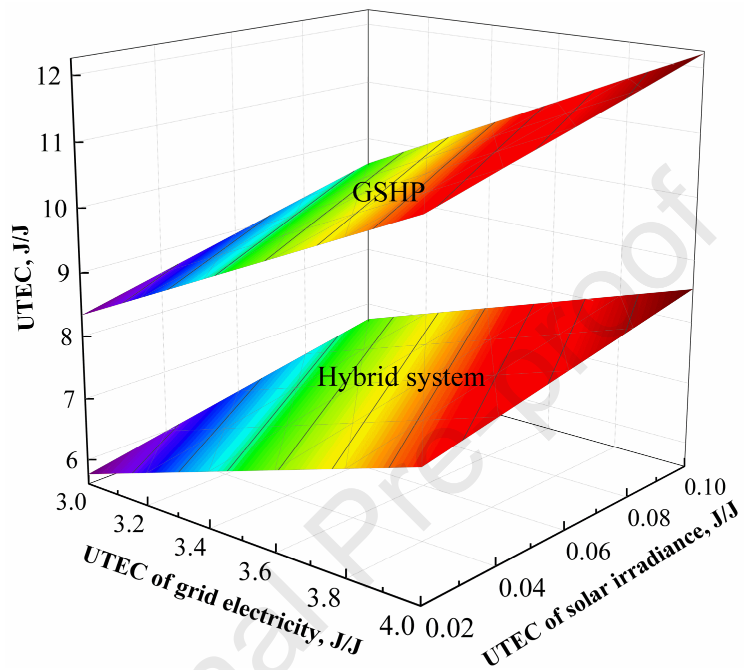

Fig. 12. UTEC of the space heating as a function of the solar irradiance and grid electricity UTEC (Red color corresponds to a higher UTEC, while blue region means a lower UTEC).

(4) Heat storage ratio and heating load

Fig. 13 illustrates how the changes in the heating load (-30% to +30%) and heat storage ratio affects the space heating UTEC. As the heat storage ratio (ε_{TES}) increases, the output of space heating water from the AHP decreases, and the GSHP supplies more space heating water by consuming also more grid electricity. As a result, the UTEC of the GSHP increases as the heat storage ratio increases. With the original heating load (0%), the heating cost of the GSHP and hybrid system raise by 0.03 J/J and 0.08 J/J, respectively when ε_{TES} increases by 0.1 units.

With an increasing heating load, the space heating water cost of the GSHP and hybrid system increases with a slowing gradient. With ε_{TES} =0.1, the cost of the GSHP and hybrid system increases by 57.43%, and 121.65% over the whole heating load range.

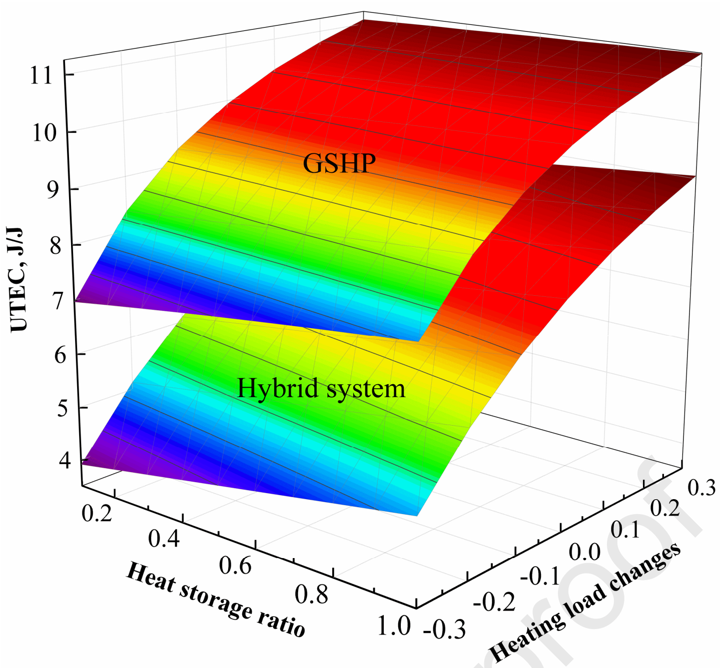

Fig. 13. Space heating UTEC as a function of the heat storage ratio and heating load change (Region in red color corresponds to a higher UTEC, while blue region means a lower UTEC).

5 Conclusions

A novel district heating system is proposed here to produce space heating water for an office building in China. The system integrates photovoltaic/thermal collector (PV/T), absorption (AHP) and geothermal (GSHP) heat pump technologies. Both energy and exergy performance of the subsystems are assessed here. A modified thermo-ecological cost (TEC) analysis method is utilized to optimize the PV/T-unit, which could be applicable for the evaluation of other integrated energy systems as well.

Comprehensive analysis and optimization of the system is performed and the key findings are presented in the following:

(1) A higher solar irradiance level would raise the solar thermal performance, and whole heating system as both solar collector outlet temperature and solar electricity output would increase. As a result, the thermodynamic performance of the integrated system would improve.

(2) Raising the PV-coverage ratio improves the energy and exergy efficiencies. This indicates that the PV would be more valuable than solar thermal for the heating system.

(3) The optimal PV-coverage ratio is found at 0.66, (66% of the PV/T unit covered by PV panels).

The optimal unit thermo-ecological cost (UTEC) of space heating water is 6.86 J/J, which is 0.05 J/J lower than the cost obtained with the conventional TEC method. To meet the full heating load, the system needs to rely on the GSHP running of grid electricity which has a high UTEC leading to a much higher heating cost with the GSHP (9.92 J/J) than with the AHP (0.19 J/J).

(4) The sensitivity analysis shows that except for the PV coverage ratio and operating hours of the PV/T unit, increasing the heating load, the heat storage ratio of the thermal tank, and UTECs of the solar irradiance and grid electricity would have a negative impact on the economic performance of heating system. The reason is that such increases would also increase the need of grid electricity with a high UTEC through the GSHP. It can be concluded that the UTEC of the hybrid heating system is sensitive to the operating condition of the GSHP. Minimizing the grid electricity use would therefore be a preferrable strategy.

Acknowledgements

This research has been supported by National Natural Science Foundation of China (Grant No. 51736006).

References

[1] Huang J, Fan J, Furbo S. Feasibility study on solar district heating in China. Renewable and Sustainable Energy Reviews. 2019;108:53-64.

[2] Ayompe LM, Duffy A, Mc Keever M, Conlon M, McCormack SJ. Comparative field performance study of flat plate and heat pipe evacuated tube collectors (ETCs) for domestic water heating systems in a temperate climate. Energy. 2011;36(5):3370-8.

[3] Allouhi A, Benzakour Amine M, Buker MS, Kousksou T, Jamil A. Forced-circulation solar water heating system using heat pipe-flat plate collectors: Energy and exergy analysis. Energy. 2019;180:429-43.

[4] Chen QF, Yuan ZX, Guo ZQ, Zhao Y. Practical performance of a small PTC solar heating system in winter. Solar Energy. 2019;179:119-27.

[5] Sinsel SR, Riemke RL, Hoffmann VH. Challenges and solution technologies for the integration of variable renewable energy sources—a review. Renewable Energy. 2020;145:2271-85.

[6] Badiei A, Golizadeh Akhlaghi Y, Zhao X, Shittu S, Xiao X, Li J, et al. A chronological review of advances in solar assisted heat pump technology in 21st century. Renewable and Sustainable Energy Reviews. 2020;132:110132.

[7] Vallati A, Ocłoń P, Colucci C, Mauri L, de Lieto Vollaro R, Taler J. Energy analysis of a thermal system composed by a heat pump coupled with a PVT solar collector. Energy. 2019;174:91-6.

[8] Kong X, Jiang K, Dong S, Li Y, Li J. Control strategy and experimental analysis of a direct-expansion solar-assisted heat pump water heater with R134a. Energy. 2018;145:17-24.

[9] Liu Z, Liu Y, Wu D, Jin G, Yu H, Ma W. Performance and feasibility study of solar-air source pump systems for low-energy residential buildings in Alpine regions. Journal of Cleaner Production. 2020;256:120735.

[10] Liu Z, Zhang Y, Xu W, Yang X, Liu Y, Jin G. Suitability and feasibility study on the application of groundwater source heat pump (GWSHP) system in residential buildings for different climate zones in China. Energy Reports. 2020;6:2587-603.

[11] Diallo TMO, Yu M, Zhou J, Zhao X, Shittu S, Li G, et al. Energy performance analysis of a novel solar PVT loop heat pipe employing a microchannel heat pipe evaporator and a PCM triple heat exchanger. Energy. 2019;167:866-88.

[12] Weeratunge H, Narsilio G, de Hoog J, Dunstall S, Halgamuge S. Model predictive control for a solar assisted ground source heat pump system. Energy. 2018;152:974-84.

[13] Sakellariou EI, Wright AJ, Axaopoulos P, Oyinlola MA. PVT based solar assisted ground source heat pump system: Modelling approach and sensitivity analyses. Solar Energy. 2019;193:37-50.

[14] Sakellariou EI, Axaopoulos PJ. Energy performance indexes for solar assisted ground source heat pump systems with photovoltaic-thermal collectors. Applied Energy. 2020;272:115241.

[15] Abu-Rumman M, Hamdan M, Ayadi O. Performance enhancement of a photovoltaic thermal (PVT) and ground-source heat pump system. Geothermics. 2020;85:101809.

[16] Sommerfeldt N, Madani H. In-depth techno-economic analysis of PV/Thermal plus ground source heat pump systems for multi-family houses in a heating dominated climate. Solar Energy. 2019;190:44-62.

[17] Xia L, Ma Z, Kokogiannakis G, Wang Z, Wang S. A model-based design optimization strategy for ground source heat pump systems with integrated photovoltaic thermal collectors. Applied Energy. 2018;214:178-90.

[18] Xia L, Ma Z, Kokogiannakis G, Wang S, Gong X. A model-based optimal control strategy for ground source heat pump systems with integrated solar photovoltaic thermal collectors. Applied Energy. 2018;228:1399-412.

[19] Chen Y, Wang J, Ma C, Shi G. Multicriteria performance investigations of a hybrid ground source heat pump system integrated with concentrated photovoltaic thermal solar collectors. Energy Conversion and Management. 2019;197:111862.

[20] Wang J, Han Z, Guan Z. Hybrid solar-assisted combined cooling, heating, and power systems: A review. Renewable and Sustainable Energy Reviews. 2020;133:110256.

[21] Szargut J. Analysis of cumulative exergy consumption. International Journal of Energy Research. 1987;11(4):541-7.

[22] Szargut Jan. Exergy method: technical and ecological applications, vol. 18. WIT press; 2005.

[23] Stanek W, Czarnowska L, Pikoń K, Bogacka M. Thermo-ecological cost of hard coal with inclusion of the whole life cycle chain. Energy. 2015;92:341-8.

[24] Stanek W, Czarnowska L, Gazda W, Simla T. Thermo-ecological cost of electricity from renewable energy sources. Renewable Energy. 2018;115:87-96.

[25] Szargut J, Stanek W. Thermo-ecological optimization of a solar collector. Energy. 2007;32(4):584-90.

[26] Stanek W, Mendecka B, Lombardi L, Simla T. Environmental assessment of wind turbine systems based on thermo-ecological cost. Energy. 2018;160:341-8.

[27] Chen Y, Wang J, Ma C, Gao Y. Thermo-ecological cost assessment and optimization for a hybrid combined cooling, heating and power system coupled with compound parabolic concentrated-photovoltaic thermal solar collectors. Energy. 2019;176:479-92.

[28] Gładysz P, Stanek W, Czarnowska L, Sładek S, Szlęk A. Thermo-ecological evaluation of an integrated MILD oxy-fuel combustion power plant with CO2 capture, utilisation, and storage – A case study in Poland. Energy. 2018;144:379-92.

[29] Stanek W, Simla T, Rutczyk B, Kabaj A, Buliński Z, Szczygieł I, et al. Thermo-ecological assessment of Stirling engine with regenerator fed with cryogenic exergy of liquid natural gas (LNG). Energy. 2019;185:1045-53.

[30] Chen Y, Wang J, Lund PD. Sustainability evaluation and sensitivity analysis of district heating systems coupled to geothermal and solar resources. Energy Conversion and Management.

2020;220:113084.

[31] EnergyPlus Energy Simulation Software.<https://www.energyplus.net/>.

[32] Wang J, Zhai Z, Jing Y, Zhang C. Influence analysis of building types and climate zones on energetic, economic and environmental performances of BCHP systems. Applied Energy. 2011;88(9):3097-112.

[33] DeST development group in Tsinghua University. Building environmental system simulation and analysis-DeST. Beijing: China Architecture & Building Press, 2006.

[34] Song Z, Wang N, You S, Wang Y, Zhang H, Wei S, et al. Integration of geothermal water into secondary network by absorption-heat-pump-assisted district heating substations. Energy and Buildings. 2019;202:109403.

[35] Wang J, Chen Y, Dou C, Gao Y, Zhao Z. Adjustable performance analysis of combined cooling heating and power system integrated with ground source heat pump. Energy. 2018;163:475-89.

[36] Wang J, Chen Y, Lior N, Li W. Energy, exergy and environmental analysis of a hybrid combined cooling heating and power system integrated with compound parabolic concentrated-photovoltaic thermal solar collectors. Energy. 2019;185:463-76.

[37] Wang J, Dai Y, Gao L, Ma S. A new combined cooling, heating and power system driven by solar energy. Renewable Energy. 2009;34(12):2780-8.

[38] F-Chart. Software, Engineering Equation Solver (EES). <http://www.fchart.com/ees/>; 2012.

[39] Arora S, Singh HP, Sahota L, Arora MK, Arya R, Singh S, et al. Performance and cost analysis of photovoltaic thermal (PVT)-compound parabolic concentrator (CPC) collector integrated solar still using CNT-water based nanofluids. Desalination. 2020;495:114595.

[40] Wang J, Yan Z, Wang M, Song Y, Dai Y. Parametric analysis and optimization of a building cooling heating power system driven by solar energy based on organic working fluid. International Journal of Energy Research. 2013;37(12):1465-74.

[41] Wang M, Wang J, Zhao P, Dai Y. Multi-objective optimization of a combined cooling, heating and power system driven by solar energy. Energy Conversion and Management. 2015;89:289-97.

[42] Wang J, Lu Z, Li M, Lior N, Li W. Energy, exergy, exergoeconomic and environmental (4E) analysis of a distributed generation solar-assisted CCHP (combined cooling, heating and power) gas turbine system. Energy. 2019;175:1246-58.

[43] Chen Y, Hua H, Wang J, Lund PD. Integrated performance analysis of a space heating system assisted by photovoltaic/thermal collectors and ground source heat pump for hotel and office building types. Renewable Energy. 2021;169:925-34.

[44] Tripathi R, Tiwari GN. Energetic and exergetic analysis of N partially covered photovoltaic thermal-compound parabolic concentrator (PVT-CPC) collectors connected in series. Solar Energy. 2016;137:441-51.

[45] Li H, Kang S, Yu Z, Cai B, Zhang G. A feasible system integrating combined heating and power system with ground-source heat pump. Energy. 2014;74:240-7.

[46] Chen Y, Wang J, Lund PD. Thermodynamic performance analysis and multi-criteria optimization of a hybrid combined heat and power system coupled with geothermal energy. Energy Conversion and Management. 2020;210:112741.

[47] Nawaz Z, Ali U. Techno-economic evaluation of different operating scenarios for indigenous and imported coal blends and biomass co-firing on supercritical coal fired power plant performance. Energy. 2020;212:118721.

[48] Wang J, Yang Y, Mao T, Sui J, Jin H. Life cycle assessment (LCA) optimization of solar-assisted hybrid CCHP system. Applied Energy. 2015;146:38-52.

[49] Jing Y-Y, Bai H, Wang J-J, Liu L. Life cycle assessment of a solar combined cooling heating and power system in different operation strategies. Applied Energy. 2012;92:843-53.

[50] Marinelli S, Butturi MA, Lolli F, Rimini B, Gamberini R. Data on the environmental performance analysis of a dual-source heat pump system. Data Brief. 2020;31:105919.

[51] Wang J, Chen Y, Lior N. Exergo-economic analysis method and optimization of a novel photovoltaic/thermal solar-assisted hybrid combined cooling, heating and power system. Energy Conversion and Management. 2019;199:111945.

[52] Stanek W, Czarnowska L. Thermo-ecological cost – Szargut's proposal on exergy and ecology connection. Energy. 2018;165:1050-9.

[53] Reklaitis GV, A. Ravindran, and Kenneth M. Ragsdell. Engineering optimization Methods and applications. New York Wiley, 1983.

Highlights

- Novel district heating system with photovoltaic/thermal collector and geothermal heat pump.
- Thermodynamic performance at various conditions.
- Modified thermo-ecological cost method to optimize the heating cost.
- Sensitivity analysis against crucial parameters.

Declaration of interests

☒ The authors declare that they have no known competing financial interests or personal relationships that could have appeared to influence the work reported in this paper.

☐The authors declare the following financial interests/personal relationships which may be considered as potential competing interests: